sciendo   Journal of Hydrology and Hydromechanics   Institute of Hydrology SAS

Correlation between climate and flood indices in Northwestern Italy at different temporal scales

Matteo Pesce[*], Jost von Hardenberg, Pierluigi Claps, Alberto Viglione

Department of Environment, Land and Infrastructure Engineering, Politecnico di Torino, Corso Duca degli Abruzzi, 24, 10129 Turin, Italy.
[*] Corresponding author. Tel.: +39 0110905606 / 5606. E-mail: matteo.pesce@polito.it

Abstract: The occurrence of river floods is strongly related to specific climatic conditions that favor extreme precipitation events leading to catchment saturation. Although the impact of precipitation and temperature patterns on river flows is a well discussed topic in hydrology, few studies have focused on the relationship between peak discharges and standard Climate Change Indices (ETCCDI) of precipitation and temperature, widely used in climate research. It is of interest to evaluate whether these indices are relevant for characterizing and predicting floods in the Alpine area. In this study, a correlation analysis of the ETCCDI indices annual time series and annual maximum flows is presented for the Piedmont Region, in North-Western Italy. Spearman's rank correlation is used to determine which ETCCDI indices are temporally correlated with maximum discharges, allowing to hypothesize which climate drivers better explain the interannual variability of floods. Moreover, the influence of climate (decadal) variability on the tendency of annual maximum discharges is examined by spatially correlating temporal trends of climate indices with temporal trends of the discharge series in the last twenty years, calculated using the Theil-Sen slope estimator. Results highlight that, while extreme precipitation indices are highly correlated with extreme discharges at the annual timescale, with different indices that are consistent with catchment size, the decadal tendencies of extreme discharges may be better explained by the decadal tendencies of the total annual precipitation over the study area. This suggests that future projections of the annual precipitation available from climate models simulations, whose reliability is higher compared to precipitation extremes, may be used as covariates for non-stationary flood frequency analysis.

Keywords: Flood tendency; ETCCDI indices; Flood and climate variability.

1 INTRODUCTION

River floods are one of the most impacting natural hazards with global annual average losses of US $104 billion (UNISDR, 2015). This estimated value is expected to increase as a consequence of population growth, urban expansion and climate change. In particular climate change is a source of concern for increasing river flooding episodes resulting from the enhanced water-holding capacity of a warmer atmosphere. In fact, large floods have occurred in Europe in the last decades; among these we can distinguish events occurring in Central Europe in 2002, 2013 and 2021 (e.g., Blöschl et al., 2013a; Kreienkamp et al., 2021; Ulbrich et al., 2003), winter floods in north-west England in 2009 and 2015/2016 (e.g., Barker et al., 2016; Miller et al., 2013), autumn floods in Northwestern Italy such as 1994, 2000 and 2016 in Piedmont (e.g., Cassardo et al., 2001; Grazzini et al., 2020) and 2011 in Liguria (Silvestro et al., 2012; Silvestro et al., 2016).

Given this evidence, many recent studies have focused on the detection of past changes in flood hazard. These studies typically use the Mann-Kendall test to detect changes in the mean annual flood magnitude and frequency (Mediero et al., 2014; Petrow and Merz (2009); Prosdocimi et al., 2014; Villarini et al., 2011). Among them, recently, Blöschl et al. (2019) analysed the most comprehensive dataset of observations in Europe (Hall et al., 2015) and found spatial patterns of trends in the annual maximum streamflow for the period 1960–2010. The detected trends were also attributed to three possible drivers of floods: the annual maximum seven-day precipitation, the highest monthly soil moisture and the spring temperature as a proxy for snowmelt and snow-to-rain

transition. This was done by analysing and correlating the long-term temporal evolution of floods and their drivers in different European hotspots. Many studies considered non-stationary flood frequency analysis to attribute flood changes to potential drivers, by modelling distribution parameters with time-varying climatic covariates (e.g., Prosdocimi et al., 2014; Prosdocimi et al., 2015; Šraj et al., 2016; Viglione et al., 2016). Bertola et al. (2020) analysed the differences between small and large flood changes (corresponding to the 2-year and 100-year floods) in Europe, paving the way for an attribution analysis, as function of the return period (Bertola et al., 2021).

Also studies analysing future flood projections typically consider changes in the magnitude of flood quantiles (e.g., Alfieri et al., 2015; Rojas et al., 2012). In Alfieri et al. (2015) an ensemble of European flood projections for different future time periods was compared with flood simulations for an historical period, used as a baseline. In that work, the projections of two possible drivers of floods such as the annual precipitation and the annual maximum daily precipitation were considered and the possible interconnections with flood change at the regional scale were analysed. Both the annual precipitation amount and the annual maximum daily precipitation are examples of standard climate indices, as defined by the Commission for Climatology/World Climate Research Programme/Technical Commission for Oceanography and Marine Meteorology (CCI/WCRP/JCOMM) Expert Team on Climate Change Detection and Indices (ETCCDI, see e.g., Zhang et al., 2005). ETCCDI indices[1] are widely used in the "climate literature" to evaluate statistics of temperature and precipitation extremes and they can be applied to study a variety of extreme events such as heavy rain, floods, droughts,

heat waves, etc. In particular, they can be important not only to analyse past climate changes, but also to characterize future changes by using projections of climate models (e.g., Sardella et al., 2020). It is of interest to evaluate whether and which ETCCDI indices are relevant for characterizing and, therefore, predicting flood changes.

This work aims at exploring the possible correlations between the annual maximum daily discharges and ETCCDI indices time series at the catchment scale in Northwestern Italy. This provides a useful indication of which extreme precipitation and temperature indices could be used as covariates for estimating annual flood probabilities and their temporal change in this region. The study area is broadly coincident with the upper part of the drainage basin of the Po River that drains the semicircle of mountains formed by the Alps and Apennines surrounding the region on three sides. It has a temperate climate with a continental character, which in the Alps becomes progressively temperate-cold and cold as altitude rises, with rainfall that falls mainly in spring and autumn on most of the territory, and in summer in the higher inland Alpine areas. It is worth considering this study area because of its heterogeneity, particularly in terms of elevation and dominance of snow related processes, leading to effects of precipitation and temperature changes on floods that are not trivial. Two types of correlation analysis are carried out: on the one hand a temporal correlation is performed at the annual time scale between maximum discharges and ETCCDI indices for each catchment, useful to capture the best covariates related to the annual variability of floods. On the other hand, in the spirit of comparative hydrology (Falkenmark and Chapman, 1989), a spatial correlation is performed among trends of maximum discharges and trends of ETCCDI indices, in order to find which covariates best explain the regional variability of the decadal tendency of floods. By focusing on multi-year tendency rather than on annual variability, this second analysis can be useful to select some ETCCDI indices as possible climate covariates of flood discharges, for regional non-stationary flood frequency analysis.

2 DATA AND METHODS
2.1 Discharge data

In this study, data from the regional stream gauge network managed by the regional environmental protection agency (Arpa Piemonte) are used[2]. From the entire database, only stations with at least 9 years of data in the period 1990–2019 are selected, i.e., 95 stations, whose records start not earlier than 1996. The sites are quite evenly distributed over the study area (Figure 1). For each station, mean daily discharges are considered to extract the annual maximum, which represents a typical flood index, as reported in recent literature on flood change (e.g., Blöschl et al., 2017; Blöschl et al., 2019). We use mean daily discharges rather than peak discharges to have a better consistency with the space-time scale of climate indices (which have been calculated with daily data on a coarse spatial grid, see Sect. 2.2). The mean daily flow is obtained by averaging the 48 half-hourly values recorded each day. We have discarded years with missing daily data over a period greater than or equal to 3 months.

Figures 2a and 2b show the dependence of the mean annual specific flood (MAF) and the coefficient of variation (CV) of annual specific floods on catchment area, respectively, in a double logarithmic plot. For completeness, the relation between catchment area and mean elevation and the data consistency as function of catchment area are reported in Figure 2c and 2d, respectively. MAF and CV show a decrease with catchment area, as expected. By fitting a linear model to the data points, thus assuming a power law relationship between the variables and catchment area, we find a similar behavior as in other studies (e.g., Lun et al., 2021; Merz and Blöschl, 2003; Merz and Blöschl, 2005). The coefficients found here for MAF (–0.136) and CV (–0.049) are indeed consistent with the one found in Lun et al. (2021) for the Alpine area (–0.208 and –0.020 respectively) but closer to values which are typical of the Atlantic region (–0.184 and –0.042 respectively). However, one should consider that the number of sites analysed here and their record lengths are much smaller than in Lun et al. (2021), thus determining a remarkable scatter.
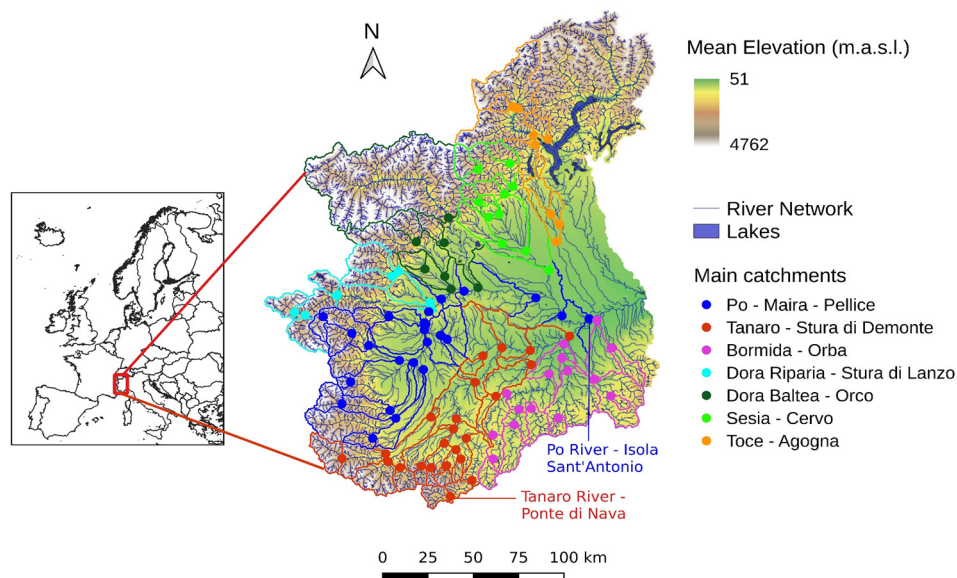

Fig. 1. Map of Piedmont region with elevation, river network, catchment boundaries and outlets colored by main rivers.
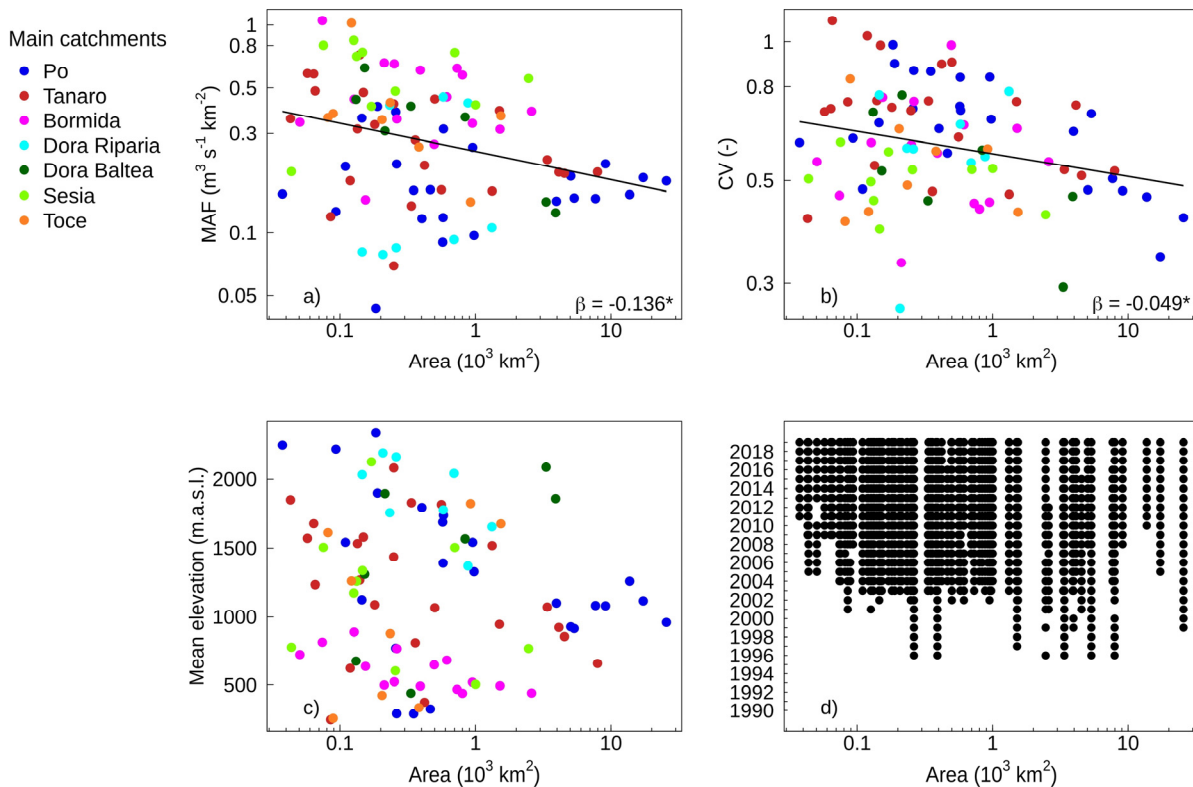
Fig. 2. a) Mean annual specific flood (MAF) vs. catchment area. b) Coefficient of variation (CV) of annual specific floods vs. catchment area, colored as in Figure 1. Lines are ordinary least squares regression lines. The values of the slope for a double logarithmic relationship are also reported. * Indicates statistical significance for a one-sided t-test at the 5% significance level. c) Area vs. mean catchment elevation. d) Data consistency vs. catchment area.

Table 1. Statistics for the 95 catchments considered in the study. Reference period: 2000–2019 (hydrologic year: 1st October 1999–30th September 2019).

	mean	CV	min	25%	median	75%	max
Area (km^2)	1596	2.32	38	146	336	951	25640
Mean elevation (m a.s.l.)	1186	0.488	244	678.5	1125	1666	2339
Mean annual precipitation (mm yr^{-1})	1095	0.210	722	932	1051	1212	1827
Mean annual runoff (mm yr^{-1})	698	0.495	148	460	644	897	1583
Aridity index (–)	0.722	0.254	0.350	0.606	0.718	0.816	1.266

2.2 Climate data for the study area

The delineated catchments are shown in Figure 1 and some statistics are reported in Table 1. These include catchment area, mean elevation, mean annual precipitation, mean annual runoff and aridity index. For the calculation of catchment area and mean elevation, a catchment extraction procedure has been performed[3], by using a digital elevation model (DEM) at 100 m resolution, obtained from data elaborated by NASA SRTM (Shuttle Radar Topography Mission) in 2000 (Farr et al., 2007). Mean annual precipitation has been calculated for each catchment by averaging the gridded precipitation values over the catchment area. Mean annual runoff has been obtained from the daily discharge values at each station in m³/s. The aridity index is provided as it is a widely used climate indicator in hydrology (Blöschl et al., 2013b). It is defined as the ratio of mean annual potential evapotranspiration and mean annual precipitation. The

potential evapotranspiration has been obtained with the modified Blaney-Criddle equation (Doorenbos and Pruitt, 1977), considering the mean daily temperature and the mean daily percentage of annual daytime hours for a latitude of 45°. The catchments cover a wide range of contributing areas and average elevations. The study area is characterized by a temperate continental climate, with significant spatial heterogeneity. In the Alps, particularly in the northern area of the region, a tendency towards more humid conditions with high precipitation amounts prevails, while the central area is experiencing more arid conditions, as shown by precipitation, potential evapotranspiration, and aridity index maps (Figure 3). It is worth noting that both the mean annual precipitation and the precipitation extremes, represented by the median and the 95th-quantile of the annual maximum daily precipitation, show the highest values in the northern part of the region. Very high precipitation extremes are also typical of the Apennines range, in the south-east.
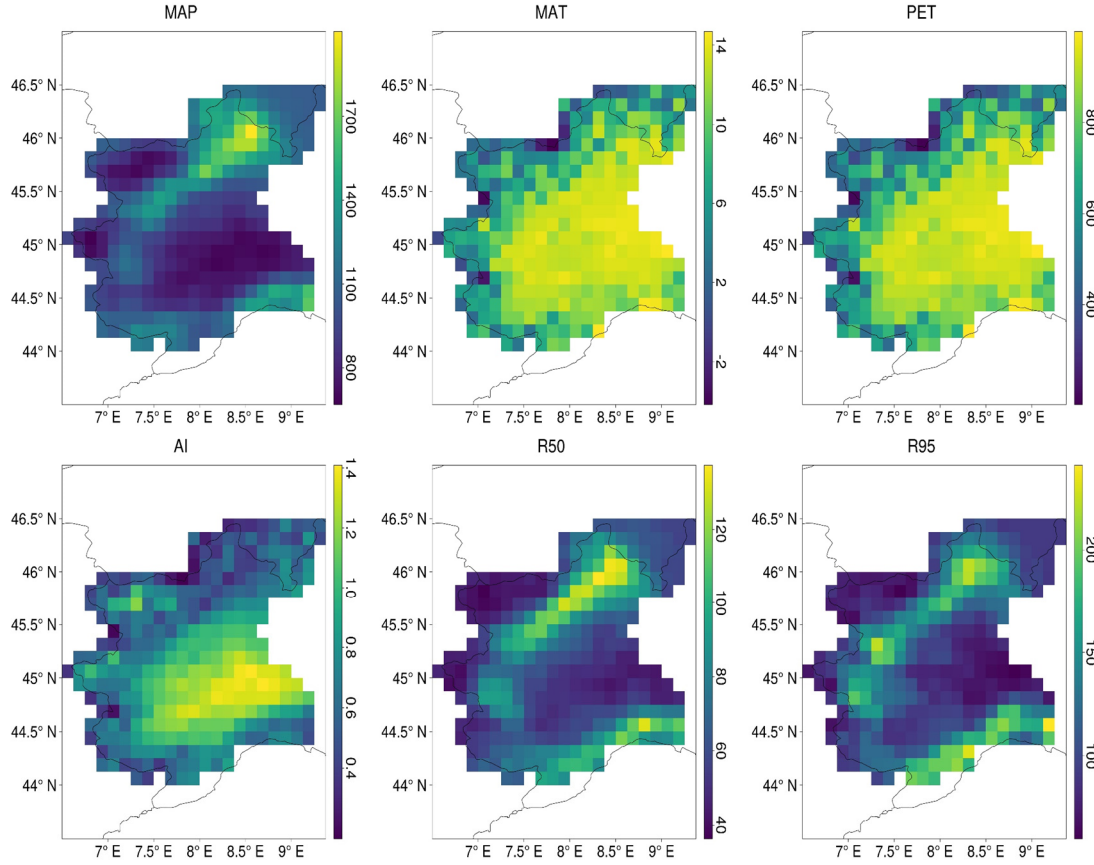
Fig. 3. Maps of the mean annual precipitation in mm/yr (MAP), temperature in °C (MAT), potential evapotranspiration in mm/yr (PET), aridity index (AI), median of the annual maximum daily precipitation in mm/d (R50) and 95th-quantile of the annual maximum daily precipitation in mm/d (R95) for the study area, derived from the Optimal Interpolation (OI) database. Reference period: 2000–2019 (hydrologic year: 1st October 1999–30th September 2019).

Daily precipitation [mm d⁻¹] and minimum and maximum daily temperature [°C] data are provided by a gridded dataset, covering the period from 01-12-1957 up to 31-12-2019, with cell resolution of 0.125° × 0.125°. This has been derived by spatial regridding through Optimal Interpolation of daily observations taken from a dense network of meteorological stations, collected by the Hydrographic Office network and by the network of the ARPA telemetry stations.[4] The Optimal Interpolation technique allows to obtain data on a regular grid homogenizing observational data from different measurement networks and sources. The data have been used for the calculation of the ETCCDI indices, which describe precipitation and temperature extremes and are widely used in climate change research (Peterson, 2005). The ETCCDI indices have been calculated at the annual timescale, with the climdex.pcic.ncdf R library, which performs an automatic calculation and saves the gridded outputs as netCDF files. Indices are referred to thresholds that are provided considering the base period 1961–1990. Both the annual maximum discharge and the ETCCDI indices refer to the hydrologic year (1st October–30th September). Gridded indices have been clipped based on catchment boundary and average annual indices at the catchment scale have been obtained. This has been done with a weighted average that considers the proportion of each pixel inside the catchments. The resulting indices annual time series have been coupled with the annual maxima of the mean daily discharges, so we consider for the analysis only years with available discharge data. The choice of a quite coarse data resolution is justified by the fact that it is consistent with outputs of regional climate models for

future projections. Moreover, we are interested in describing regional floods, not local flash floods.

2.3 Correlation measures

Spearman's rank correlation is applied to annual data to inspect which indices have the highest temporal correlation with annual maximum daily discharges. The choice of the Spearman correlation instead of other statistical measures of association between variables (e.g., Pearson correlation) is due to the expected non-linear relationship between precipitation, temperature, and discharge. Starting from the common definition of the Pearson's correlation coefficient between two variables (x and y):

$$r_{x,y} = \frac{1}{n-1} \sum_{i=1}^{n} \left(\frac{x_i - \bar{x}}{\sigma_x} \right) \left(\frac{y_i - \bar{y}}{\sigma_y} \right) = \frac{\text{cov}(x,y)}{\sigma_x \sigma_y} \tag{1}$$

where n is the number of observations, $\bar{x}$ and $\bar{y}$ are the mean values of x and y, σ_x and σ_y are the standard deviations of x and y, the Spearman's correlation coefficient is defined as the Pearson correlation coefficient between the ranks (Rx and Ry) of the variables:

$$\rho_{Rx,Ry} = \frac{\text{cov}(Rx, Ry)}{\sigma_{Rx} \, \sigma_{Ry}} \tag{2}$$

where $\text{cov}(R_x, R_y)$ is the covariance of the rank variables, and σ_{Rx} and σ_{Ry} are the standard deviations of the rank variables. By substituting the ranks into Equation (1) and simplifying, the

coefficient can be computed with the following formulation, which exactly holds in case of no ties (Helsel et al., 2020), Chapter 8.3):

$$\rho = \frac{\sum_{i=1}^{n}(Rx_i \, Ry_i) \; - \; n\left(\frac{n+1}{2}\right)^2}{n(n^2-1)/12} \tag{3}$$

The test statistic used for testing the significance of ρ under the null hypothesis of no-correlation between the variables is defined as:

$$S = \sum_{i=1}^{n}(Rx_i - Ry_i)^2 = (1-\rho)(n^3-n)/6 \tag{4}$$

with the right-hand formulation holding in case of no ties. For small sample sizes ($n < 20$), the algorithm AS 89 (Best and Roberts, 1975) is used to compute exact p-values, by calculating the discrete probability distribution associated with S. For n < 10, p-values are exact, while for larger sample size an Edgeworth series approximation is used. For large sample sizes ($n > 20$), the test can be computed on the transformed variable:

$$t = \frac{\rho \sqrt{n-2}}{\sqrt{1-\rho^2}} \tag{5}$$

where n is the length of the two tested samples and t is distributed as a Student's t-distribution with $n-2$ degrees of freedom, under the null hypothesis of no-correlation between the variables (Helsel et al., 2020, Chapter 8.2). In this case, p-values are calculated as:

$$p = 1 - F_t(\mathrm{abs}(t), n-2) \tag{6}$$

where $F_t(\mathrm{abs}(t), n–2)$ indicates the non-exceedance probability associated with the quantile abs(t) for a Student's t-distribution with $n–2$ degrees of freedom. In the presence of ties, this is the approach adopted for the calculation of p-values. We consider one-sided tests at 5% significance level, both for positive and negative correlation.

Confidence intervals of the correlation are found by using the Fisher z transform of the correlation:

$$z = \frac{1}{2}\ln\left(\frac{1+\rho}{1-\rho}\right) = \mathrm{arctanh}(\rho) \tag{7}$$

and then assuming z as normally distributed with standard deviation:

$$\sigma_z = \sqrt{\frac{1}{n-3}} \tag{8}$$

The values are finally back transformed to obtain confidence intervals in correlation units.

The same procedure is also applied to detrended data, to check for the impact of the presence of trends in the data on the annual correlation among maximum discharges and climate indices. For this purpose, the Theil-Sen linear regression model with time, which is widely discussed in the following section 2.4 in the context of tendency detection, is considered. The detrending has been performed for each catchment by subtracting the predicted values according to the fitted model to the observed values. Then, the correlation has been calculated on the obtained residuals. For each index, a regional mean Spearman's correlation coefficient is provided, taking into account the uncertainty associated with the single correlation values. A weighting procedure is adopted to weight the values for their confidence bounds. In particular, the weights are given by (upper bound – lower bound)$^{-1}$.

The Spearman's rank correlation is also used to evaluate the correlation among decadal tendencies of annual maximum discharges and tendencies of climate indices. This choice is justified by its application in previous studies, with the aim of studying the correlation among the tendency of discharge maxima and climate variables (e.g., Blöschl et al., 2019).

2.4 Tendency measures

The possible presence of decadal tendencies in the data is inspected for both the annual maximum discharge and climate indices. For this purpose, the Theil-Sen model is adopted, as defined by Theil (1950), with further investigations by Sen (1968). This is a robust nonparametric linear regression model of the form:

$$\hat{y} = \alpha + \beta \cdot x \tag{9}$$

In this case, the slope estimator (β) represents the median of the slopes calculated for all possible pairs of values assumed by the variable over different years:

$$\beta = \mathrm{median}\left(\frac{y_j - y_i}{j - i}\right), i < j \tag{10}$$

where y refers to the annual values of the variable, while i, j refer to different years. In this paper, the decadal tendencies will be plotted as the percentage of the mean value of the variable per year (i.e., $100 \cdot \beta/\mathrm{mean}$). The intercept ($\alpha$) of the regression line is calculated according to the approach described in Conover (1999):

$$\alpha = y_{\mathrm{med}} - \beta \cdot x_{\mathrm{med}} \tag{11}$$

where x_{med} and y_{med} are the medians of x and y, which in this case represent time and the considered variable, respectively.

We evaluate the significance of the trends with one-sided Mann-Kendall tests at the 5% significance level. The test statistic is calculated by computing the sum of the sign of differences for all $\frac{n(n-1)}{2}$ possible combinations of the n observations:

$$S = \sum_{i=1}^{n-1}\sum_{j=i+1}^{n}\mathrm{sgn}(x_j - x_i)$$

$$\mathrm{sgn}(x_j - x_i) = \begin{cases} +1, & \text{if } (x_j - x_i) > 0 \\ 0, & \text{if } (x_j - x_i) = 0 \\ -1, & \text{if } (x_j - x_i) < 0 \end{cases} \tag{12}$$

For $n \geq 10$ (Kendall, 1975), the normal approximation test can be used. The test statistic Z is defined as follow:

$$Z = \begin{cases} \dfrac{S-1}{\sqrt{\mathrm{var}(S)}}, & \text{if } S > 0 \\ 0, & \text{if } S = 0 \\ \dfrac{S+1}{\sqrt{\mathrm{var}(S)}}, & \text{if } S < 0 \end{cases} \tag{13}$$

with var(S) being the variance of S:

$$\mathrm{var}(S) = \frac{n(n-1)(2n+5) - \sum_{j=1}^{g} t_j(t_j-1)(2t_j+5)}{18} \tag{14}$$

In the formula, g represents the number of groups of tied values and t_j the number of ties in group j. In case of no ties the formulation reduces to:

$$\mathrm{var}(S) = \frac{n(n-1)(2n+5)}{18} \tag{15}$$

Z is distributed as a standard normal distribution under the null hypothesis of no trend of the variable (Mann, 1945). $Z > 0$ indicates an increasing trend and vice versa. p-values for one-sided tests are computed as the exceedance probability associated with Z.

Besides the test, we also compute confidence intervals for β, as measure of the uncertainty in the trends estimation, by selecting the upper and lower limits within the sample of ranked slopes. In particular, according to Hollander and Wolfe (1999), the critical value is given by the quantile of the standard normal distribution $z_{\frac{\alpha}{2}}$, where α is the confidence level, and the upper and lower ranks of the slopes corresponding to the confidence bounds are found by:

$$R_u = \frac{N + z_{\frac{\alpha}{2}}\sqrt{\text{var}(S)}}{2} + 1$$

$$R_l = \frac{N - z_{\frac{\alpha}{2}}\sqrt{\text{var}(S)}}{2} \qquad (16)$$

where $N = \frac{n(n-1)}{2}$ is the number of computed slopes. The

confidence level chosen for this study is 0.10, which is coherent with the Mann-Kendall test at the 5% significance level applied for positive and negative trends separately. Also for tendency estimation, a regional mean tendency is provided, taking into account the uncertainty associated with the single tendencies. The weights are given by exp(–k(upper bound – lower bound)), with $k = 0.25$, to constrain the weights range in case of confidence range equal to 0 (this is the case for the Growing season length index (GSL) in some catchments).

3 RESULTS
3.1 Temporal correlation of annual climate and flood indices

A selection of climate indices, broadly coincident with the most relevant ones in terms of results, together with the flood series for 2 catchments with different topographic characteristics are shown in Figure 4. The selected indices are the maximum 5-day precipitation (Rx5day), maximum 1-day precipitation (Rx1day), annual total precipitation when daily precipitation is above the 99th percentile (R99pTOT), annual total precipitation
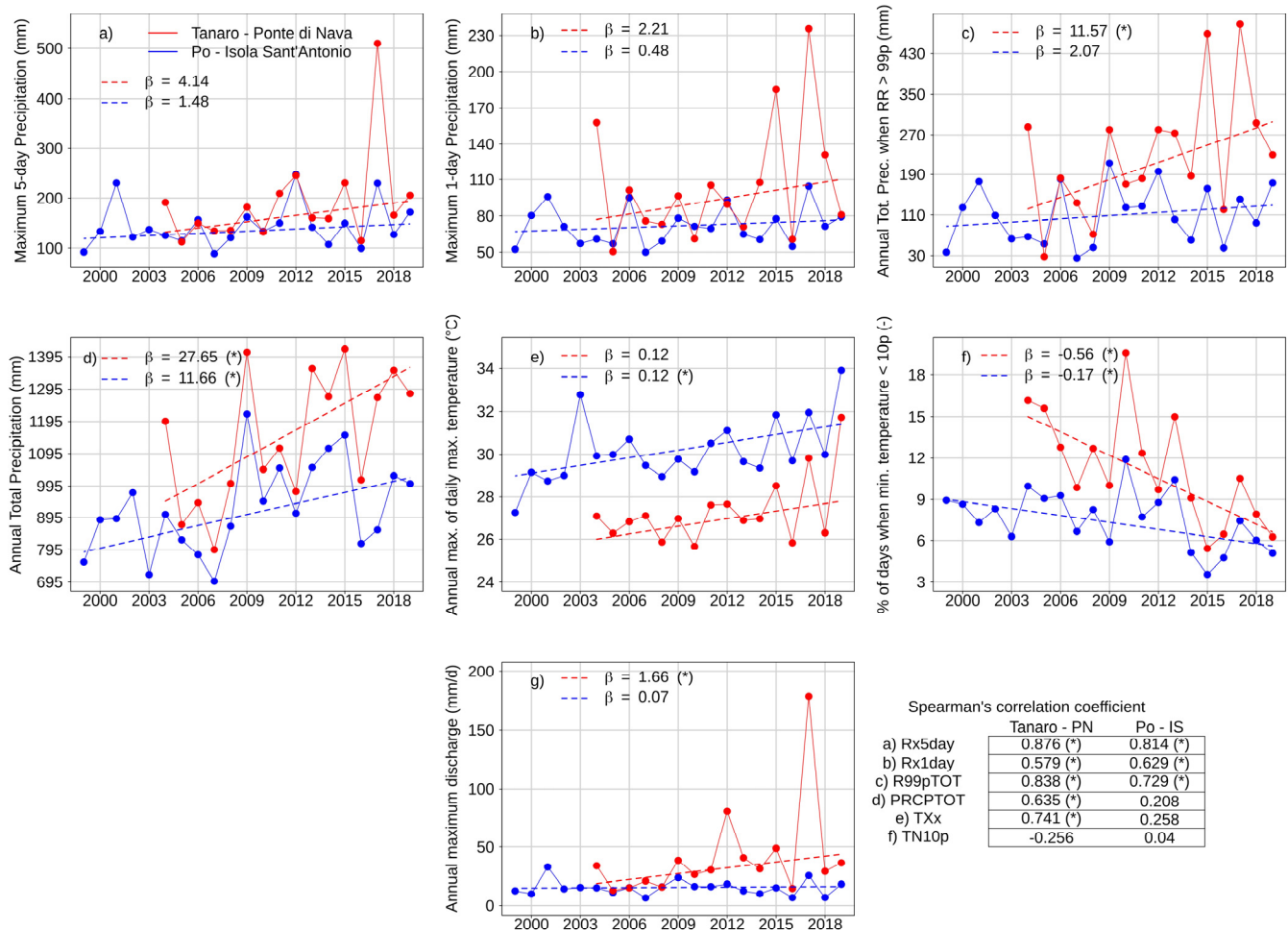

Fig. 4. A selection of climate indices and annual river flood series for 2 catchments, whose position is shown in Figure 1: the Po River catchment at Isola Sant'Antonio (area 25640 km², mean elevation 959 m a.s.l.) and the Tanaro River catchment at Ponte di Nava (area 149 km², mean elevation 1580 m a.s.l.). The represented indices are a) maximum 5-day precipitation (Rx5day), b) maximum 1-day precipitation (Rx1day), c) annual total precipitation above the 99th percentile (R99pTOT), d) annual total precipitation (PRCPTOT), e) annual maximum value of daily maximum temperature (TXx) and f) % of days when daily minimum temperature < 10th percentile (TN10p). Annual maximum discharges are in panel g). The inset shows the Spearman's rank correlation among the climate indices and discharge maxima; in this table * indicates statistically significant correlation according to one-sided tests (α = 0.05). The regression lines indicating the decadal tendency of the indices are also reported in panels a–g, together with the estimated slopes (β); in this case, * indicates statistically significant tendencies according to one-sided Mann-Kendall tests at 5% significance level.

(PRCPTOT), annual maximum value of daily maximum temperature (TXx) and % of days when daily minimum temperature < 10th percentile (TN10p). We consider the Tanaro River catchment at Ponte di Nava, a small catchment in the Southern Alps, and the Po River catchment at Isola Sant'Antonio, which is the largest lowland catchment of our dataset. The inset table provides the correlation coefficients among these indices and discharge maxima; for both stations the highest significant correlations are found for Rx5day and R99pTOT. Trends lines show the decadal tendencies of climate indices and discharge maxima in the two catchments. It appears that tendencies of climate indices are more pronounced for the high-elevation catchment, with significant results according to one-sided Mann-Kendall tests (α = 0.05) for R99pTOT, PRCPTOT, TN10p. Even the peak flows show a significant increasing trend (α = 0.05), opposed to a null tendency for the Po catchment.

More generally, this section presents the results of the correlation among the annual time series of ETCCDI indices and the annual maximum discharges. The calculation has been performed both for original and detrended data (detrended using the Theil-Sen linear regression model with time) with similar outcomes, indicating that the analysis is quite robust and is not affected by the presence of possible trends in the data (Tables A1–A4). The Spearman's rank correlation coefficients for the indices with the highest mean regional correlation are reported in Figure 5. As expected, annual maximum daily discharges are best correlated to indices of precipitation extremes: the annual maximum 1-day precipitation (Rx1day), the annual maximum consecutive 5-day precipitation (Rx5day), the annual total precipitation when daily precipitation is above the 95th daily percentile (R95pTOT) and the annual total precipitation when daily precipitation is above the 99th daily percentile (R99pTOT).
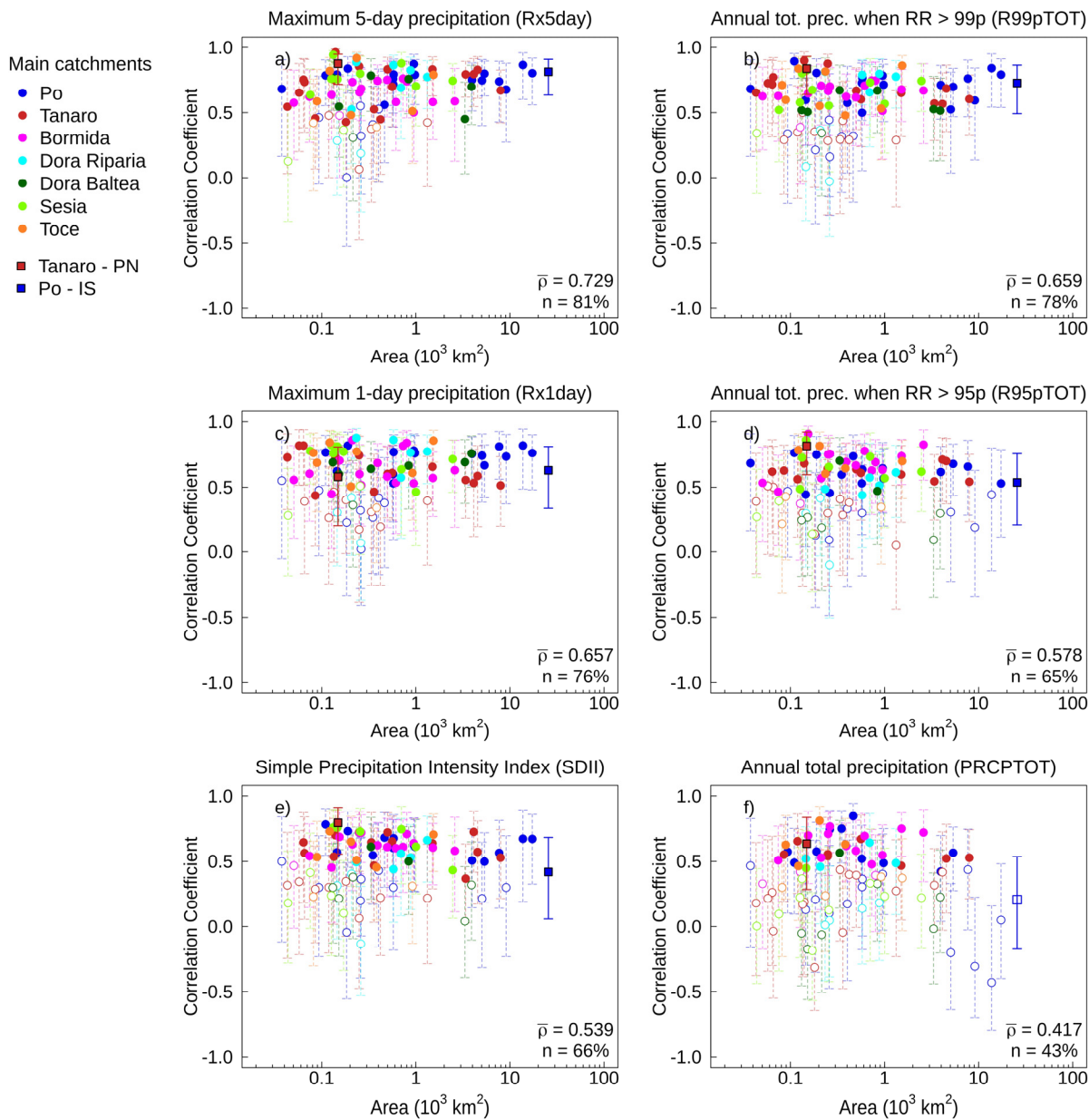

Fig. 5. Spearman's rank correlation coefficients among annual maximum mean daily discharges and a) maximum 5-day precipitation (Rx5day), b) annual total precipitation above the 99th percentile (R99pTOT), c) maximum 1-day precipitation (Rx1day), d) annual total precipitation above the 95th percentile (R95pTOT), e) simple precipitation intensity index (SDII), f) annual total precipitation (PRCPTOT) for all catchments vs. catchment area, colored as in Figure 1. For each index, the regional mean correlation coefficient and the percentage of significant cases (one-sided tests at 5% level), are reported. Full dots represent catchments with significant positive correlation, while empty dots represent not significant positive correlation. Points corresponding to the catchments described in Figure 4 are drawn as squares.

Indices related to average conditions such as the simple precipitation intensity index (SDII) and the annual total precipitation (PRCPTOT) show a lower mean correlation. Figure 5 suggests that the strength of the correlation may depend on catchment area. For example, the annual maximum consecutive 5-day precipitation shows higher correlation compared to the annual maximum 1-day precipitation for large catchments (A > 2000 km²), while the opposite occurs for the small ones (A < 100 km²). Moreover, it can be observed that R99pTOT is more significantly correlated to the maximum discharges than R95pTOT, in particular for medium-to-large sized catchments (A > 500 km²). Considering the annual total precipitation, the correlations are weaker compared to the other indices, and no significant correlation can be established for very large catchments, which are typically the Po River catchments located in the central lowland area. For temperature indices, instead, the correlation values are generally lower and significant for a smaller number of catchments (Tables A2 and A4).

3.2 Decadal tendency of climate and flood indices

In order to investigate whether the decadal tendency of the flood magnitudes depend on the same climate indices which are relevant to explain the annual floods, the trends of both ETCCDI indices and discharge maxima have been calculated over the period 2000–2019, and then a spatial correlation analysis of the trends of the variables has been performed. In other words, we evaluate whether the spatial variability of the trends (i.e., multi-annual tendency) in the ETCCDI indices explains the spatial variability of the trends in the annual maximum daily discharges in the Piedmont Region.

The estimated trends in the annual maximum discharges are presented in Figure 6. Floods don't show a dominant tendency at the regional scale and some noise appears in the data mainly due to the limited length of the time series (7% of the sites have a significant trend according to one-sided Mann-Kendall tests at the 5% significance level). Since many stations are located on the same river from upstream to downstream, some spatial coherence of the tendency sign, according to the geographical location, can be observed. A positive tendency is dominant in most Bormida and Tanaro catchments, located in the southwest area (pink and red points in Figure 6, respectively), while in other catchments the situation is more heterogeneous. Looking at Po River, for example, the tendency is negative for small catchments, which are typically located in the western Alps, while for medium-sized hilly catchments it is positive. Finally, there is no clear tendency for the largest valley catchments. Negative trends can be observed also in the smallest Sesia catchments, located in the northern Alpine area.

Significant tendencies are instead found for most ETCCDI indices, more so for temperature indices than precipitation ones. The main results for precipitation indices are reported in Figure 7. As can be noted, the trends are mainly positive and extreme indices such as R99pTOT and R95pTOT show a decreasing tendency for increasing catchment area. This is particularly the case for the Po River catchments (blue points). Total precipitation shows one of the clearest pattern as it is experiencing a positive significant tendency in around 50% of the catchments (Table A5), but the spatial variability does not seem to depend on catchment area. The number of days with precipitation above 20 mm (R20mm), together with Rx5day and Rx1day show a certain spatial homogeneity, thus indicating that they may not be ideal in explaining the spatial variability of flood decadal tendencies, as investigated in the next section 3.3.
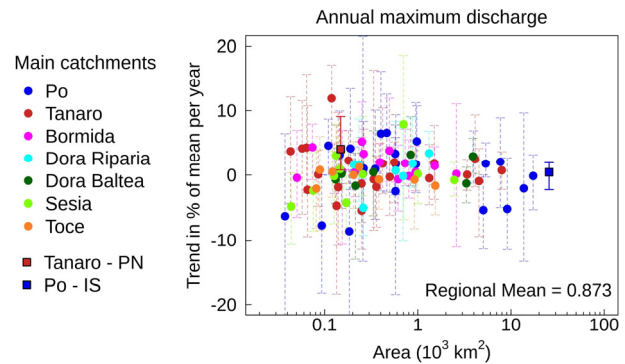

Fig. 6. Trends of annual maximum mean daily discharge for each catchment vs. catchment area, colored as in Figure 1. The regional mean trend is also reported. Points corresponding to the catchments described in Figure 4 are drawn as squares.

The most relevant results for temperature indices are instead shown in Figure 8. The % of cold days (TX10p) and the % of cold nights (TN10p) show a marked negative tendency in almost all catchments. These indices also show a spatial pattern that depends on the area, since the tendency increases for increasing catchment area, meaning that the intensity of the warming tendency actually reduces for increasing area. Trends of the annual maximum of minimum temperature (TNx), annual maximum of maximum temperature (TXx) and the growing season length (GSL) are also reported. For these indices the relative trend magnitude appears to be lower and there is not a clear spatial variability, but they show a significant relationship with flood trends that will be discussed in the next section.

3.3 Correlation of decadal tendencies of climate and flood indices

The main results of the spatial correlation analysis among decadal tendencies of ETCCDI indices and decadal tendencies of annual maximum discharge are shown in Figure 9, where mean catchment elevation is also reported through circle sizes.

Concerning precipitation indices, the total annual precipitation (PRCPTOT) tendency shows the highest significant correlation, according to a one-sided test at 5% significance level, with a Spearman correlation coefficient of 0.500, followed by the annual maximum consecutive 1-day precipitation (Rx1day) and the annual total precipitation exceeding the 99th daily percentile (R99pTOT). This indicates that the long-term variability of floods seems to be better explained by mean precipitation, rather than by indices of extreme precipitation.

The analysis on temperature indices provides a significant positive correlation ($\rho = 0.277$) with the tendency of the growing season length (GSL) and a negative correlation with the tendency of the maximum value of the daily maximum temperature (TXx) and maximum value of the daily minimum temperature (TNx), with the coefficients equal to –0.310 and –0.215, respectively. Since the tendencies of these indices show a limited spatial variability, as revealed by Figure 8, the results obtained for temperature indices may be spurious. Anyway, the negative correlations among the tendencies of discharge maxima and the maximum value of daily temperatures may be of interest from a hydrologic point of view. Some tests, which are not presented here, have revealed that by considering only
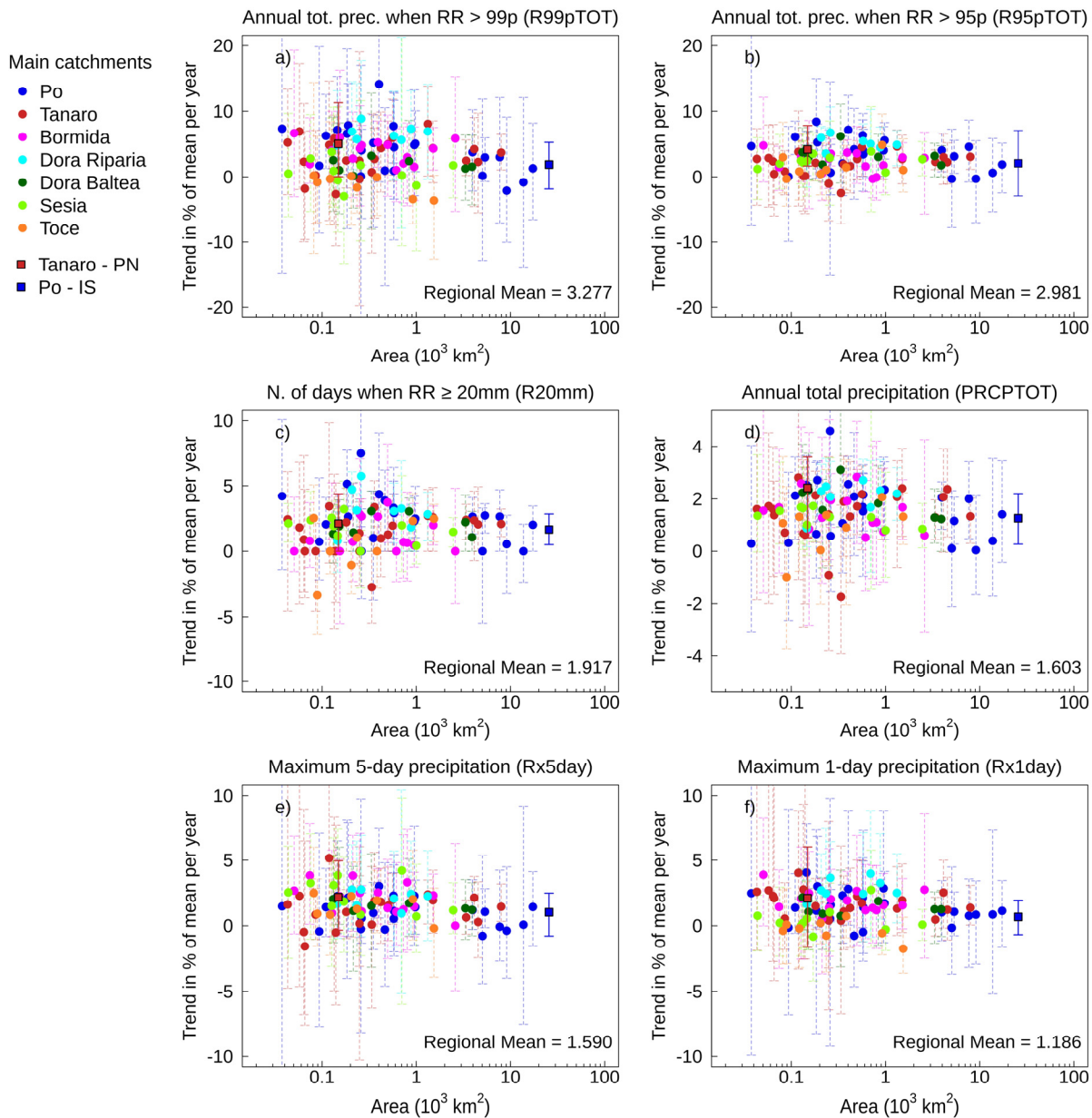
Fig. 7. Trends of a) annual total precipitation above the 99th percentile (R99pTOT), b) annual total precipitation above the 95th percentile (R95pTOT), c) annual number of days when precipitation is above 20 mm (R20mm), d) annual total precipitation (PRCPTOT), e) maximum 5-day precipitation (Rx5day), f) maximum 1-day precipitation (Rx1day), for each catchment vs. catchment area, colored as in Figure 1. For each index, the regional mean trend is reported. Points corresponding to the catchments described in Figure 4 are drawn as squares.

catchments at medium-to-high elevation (> 1500 m), the absolute value of correlation coefficients for these indices increase and this can also be grasped from Figure 9. This suggests that the results for temperature indices are mainly driven by high elevation catchments, where snow-related processes dominate in the formation of floods, which are typically in the spring season.

4 DISCUSSION AND CONCLUSIONS

In this study, we correlate annual maximum daily discharges with standard climate indices (ETCCDI) at the catchment scale, over the period 2000–2019. A temporal correlation analysis conducted at the annual scale, to evaluate which indices better explain annual discharge maxima, is followed by a spatial correlation of the tendencies of annual maximum discharges

and climate indices time series, with the aim of explaining the multi-annual tendency of floods in terms of climatic drivers.

The temporal correlation analysis indicates that indices of extreme precipitation (Rx5day, Rx1day, R99pTOT, R95pTOT) are highly positively correlated to annual streamflow maxima, more than indices of mean precipitation. In particular, R99pTOT seems to be more suitable to describe annual maximum discharges compared to R95pTOT. This can be explained by the fact that the former is considering a very high precipitation threshold so is a good proxy for the annual maximum flow events, while the latter incorporates rainfall events not necessarily leading to the largest flood peak. For this reason, R95pTOT could be used to describe other indicators of extreme discharge (e.g., flow volumes, not considered in this study). Another interesting result follows from the comparison between the maximum 1-day precipitation (Rx1day) and the maximum
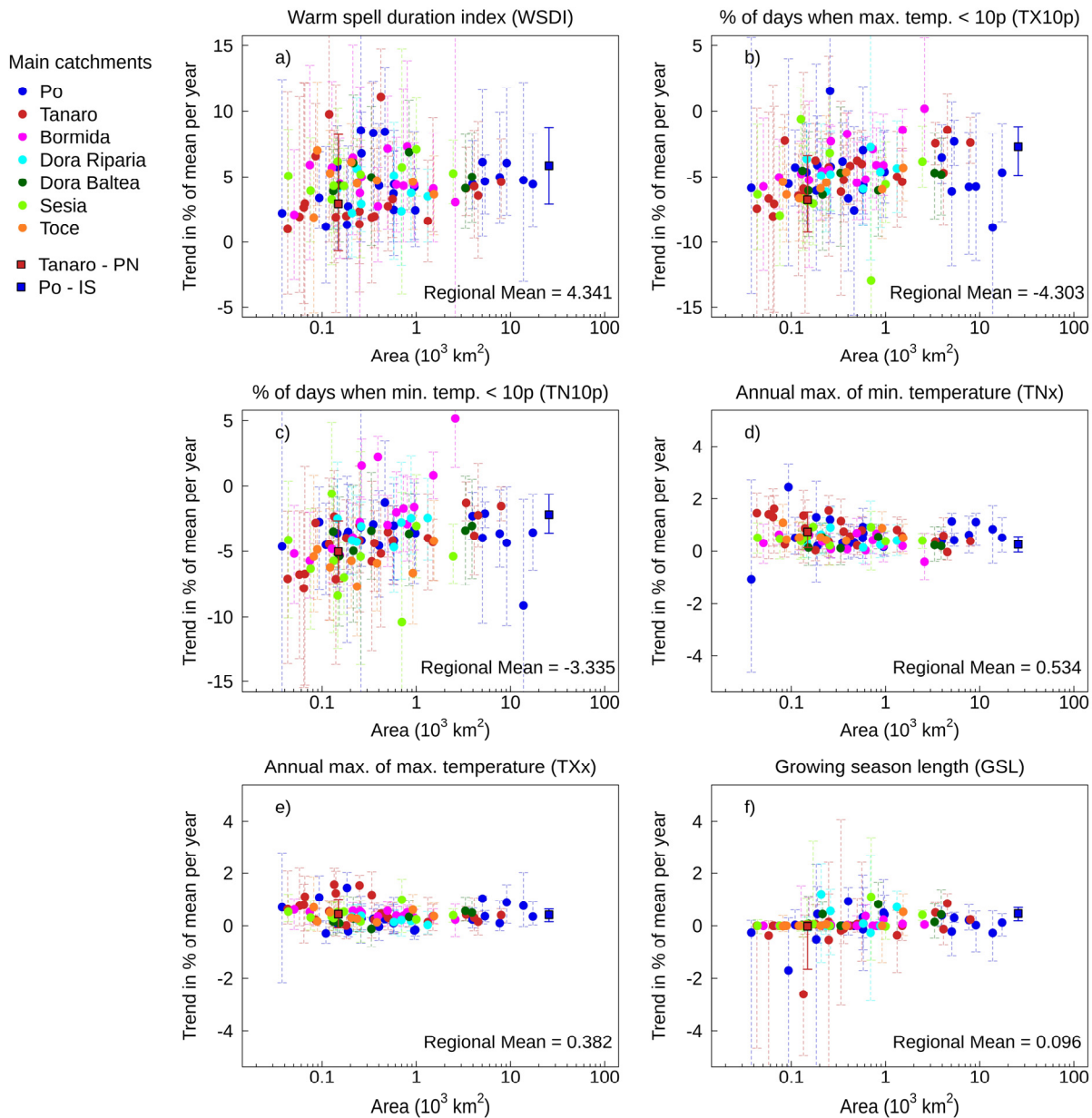
Fig. 8. Trends of a) warm spell duration index (WSDI), b) % of days when the maximum temperature is lower than the 10th percentile (TX10p), c) % of days when the minimum temperature is lower than the 10th percentile (TN10p), d) maximum value of daily minimum temperature (TNx), e) maximum value of daily maximum temperature (TXx), f) growing season length (GSL) for each catchment vs. catchment area, colored as in Figure 1. For each index, the regional mean trend is reported. Points corresponding to the catchments described in Figure 4 are drawn as squares.

5-day precipitation (Rx5day). Rx1day shows higher correlation to annual maxima for small catchments, while Rx5day seems to perform better for large catchments. This is mainly due to the interplay between the duration of rainfall events and the catchment response time. In fact, it's well known that longer (shorter) precipitation events are relevant in determining floods in larger (smaller) catchments. The majority of catchments with intermediate size (i.e., 100 km² < A < 600 km²) don't show high correlation values for both Rx1day and Rx5day indices, as well as for other extreme indices. A possible way to improve the results for intermediate-sized catchments could be to use some ad-hoc indices, to capture rainfall events having a timescale more relevant for these catchment sizes. An example is the maximum consecutive 3-day precipitation (Rx3day), which has not been considered here since it is not part of the standard ETCCDI indices.

A trend analysis of all variables has been performed to conduct the spatial correlation analysis. This is done because of the limited record length of the data. With long data records, one could temporally correlate the 10-year moving averages (or non-overlapping blocks) extracted from the series of discharge maxima and climate indices. Here we assume that an indication on which indices are better correlated to flood annual maxima can be obtained seeking for those indices whose tendency is correlated in space (for the different catchments) with the tendency of the flood themselves. In other words, we identify the ETCCDI indices that better explain the flood tendencies at a regional level, while the procedure cannot identify those indices that better explain the flood tendencies at a sub-regional or local level.

The trend analysis applied to the data highlights some limitations in terms of the statistical significance of the differences within the region, i.e., the estimated trends are often overlapping
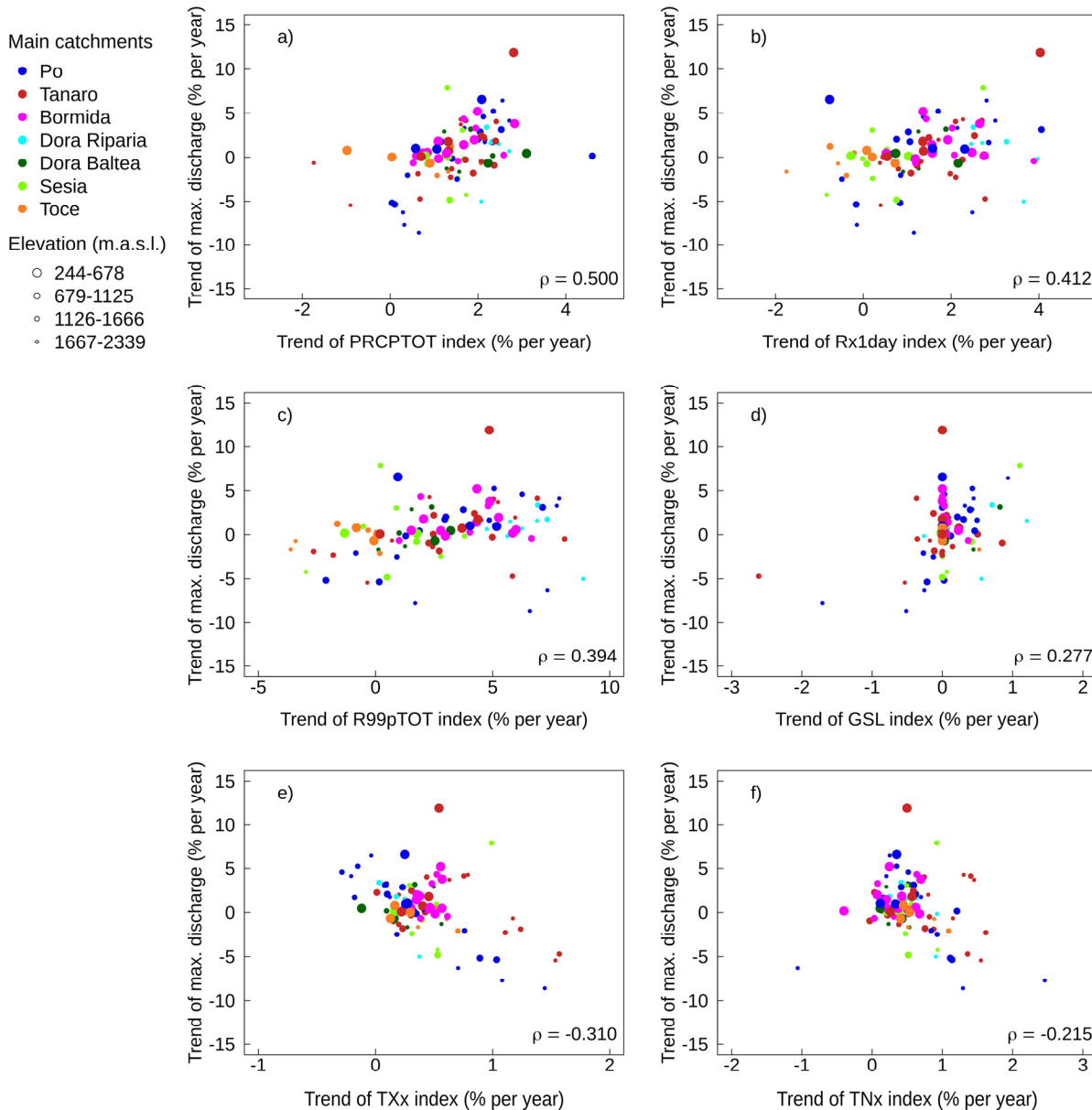
Fig. 9. Trends of annual maximum mean daily discharges vs. trends of a) annual total precipitation (PRCPTOT), b) maximum 1-day precipitation (Rx1day), c) annual total precipitation above the 99th percentile (R99pTOT), d) growing season length (GSL), e) maximum value of daily maximum temperature (TXx), f) maximum value of daily minimum temperature (TNx), discretized by mean catchment elevation, colored as in Figure 1. Spearman's rank correlation coefficients are reported.

if one considers the uncertainty associated with them. This is visible observing the tendencies in the flood discharges and climate indices and can be mainly attributed to the limited length of the series (15 years, on average). Nonetheless, it is worth noting that finding trends which are significantly different from zero is not really relevant for the outcomes of the analysis, since the main goal is to check for a coherent tendency correlation of climate and flood indices, considering all sites. For this reason, the spatial correlation analysis is still useful for attributing the flood tendency variability characterizing the study region.

Looking more closely at the results, it appears that, as already mentioned, the highest correlation is found for the annual total precipitation which represents mean precipitation conditions. This result suggests that, while extreme precipitation is highly correlated with extreme discharges at the annual timescale, as one would expect from a mechanistic model of the

hydrologic response, the decadal changes of extreme discharges may be better explained by the decadal changes of the average precipitation. This is related to the role played by average precipitation on catchment saturation, as demonstrated by other studies (see e.g., Šraj et al., 2016). Besides, the average or total precipitation is itself correlated to extreme precipitation.

Temperature indices tell us that the tendency of annual maximum daily temperatures show a negative correlation to flood tendencies, at least for high elevation catchments. There is a likely connection between temperatures and snowmelt and ice melt dynamics; higher summer temperatures are responsible of the retreat of glacierized areas and can be themselves correlated to the occurrence of longer dry periods in the mountains, which don't favor the process of snow accumulation, as has been observed in the Alps in the last 20 years (Beniston et al., 2018). This can result in a negative tendency of runoff peaks, which in these catchments typically occur during late spring or summer.

A thorough analysis on the type of events occurring (e.g., to analyse the impact of rain-on-snow events) could be useful to better attribute the evolution of annual discharge maxima at high elevation.

The large uncertainties in the tendencies of the indices, mainly due to the record length and the size of the region, should be a warning on the fact that the correlations identified in our spatial correlation analysis may be spurious. In other words, from a statistical point of view, the regional differences of the indices are not strong. To deal with the presence of possible spurious correlations, more robust approaches could be used that also account for the expected sensitivity of the long term flood behavior to the covariates, such as the method in Bertola et al. (2019). From a hydrologic perspective, regional differences in precipitation and temperature tendencies are possible. Libertino et al. (2019) found trends of annual maxima of precipitation over Italy, for different durations and at different spatial scales. Considering Northwestern Italy, trends showed some variability for different areas of the region, with the presence of significant positive/negative trends in hilly or mountainous stations opposed to a not distinct pattern over the Po valley for 12 h and 1-day precipitation. Even though the time period considered is different, this is consistent with the results obtained here for indices of precipitation intensity such as Rx1day and R99pTOT. Also, in terms of frequency of extremes, our study suggests an overall increase of the annual number of days with precipitation above 20 mm (R20mm) for small and medium-sized catchments, and this seems to be in continuity with the increasing annual record breaking anomaly found in Libertino et al. (2019) for the upper Po Region, during the late '80s–early '90s. Temperature trends found in this study reveal a strong relative decrease of the % of cold days and cold nights (TX10p and TN10p), which is more exacerbated in small catchments, typically located at high elevation in the Alps (Figure 8b and 8c), and this is in accordance with previous studies on climate trends in this area (see e.g., Acquaotta et al., 2015). Moreover, also warm days and warm nights (TX90p and TN90p) show an overall significant regional increasing tendency (Table A6), in continuity to what found by Fioravanti et al., 2016, both for Piedmont region and at the national scale. Regarding that study, we would like to point out that the poorly significant results obtained for the period 1961–1977, compared to other longer time periods, confirm that the length of the time series can be critical for the outcomes of the Mann-Kendall test, but, as they reported, some useful indications in terms of decadal tendencies can still be provided.

The analysis performed here is not multivariate and therefore is not able to capture and quantify the relative contribution of temperature and precipitation indices in explaining flood tendencies. For mountain regions like Piedmont this could be expected and other statistical tools such as machine learning techniques (e.g., Random forest) or, more generally, conceptual models could be used to quantify the relative importance of different explanatory variables (see e.g., Bertola et al., 2021; Zeng et al., 2021). Nevertheless, the results obtained here provide a first order indication of which ETCCDI indices may be related to floods.

Considering the results for precipitation indices, also Zeng et al. (2021) identified total precipitation as the most important driver of streamflow change in the U.S., confirming the dominant role of climate in determining the hydrologic regime. The main implication of this study is that future projections of mean precipitation for the Alpine area, obtained from running state-of-the-art climate models, may be used as covariates in non-stationary flood frequency analysis, to produce flood change projections in terms of intensity and frequency. The uncertainty associated with climate models projections is very high and this is largely reflected in the prediction of flood changes, in particular for scenarios towards the end-of-century. In this respect, it's worth noting that the inherent uncertainty of projections of annual total precipitation is lower compared to the uncertainty related to extreme precipitation, which leads to some issues in the representation of extremes (Alfieri et al., 2015). For this reason, the use of total precipitation as covariate can favor more reliable future flood estimates.

REFERENCES

[1]http://etccdi.pacificclimate.org/list_27_indices.shtml
[2]https://www.arpa.piemonte.it/rischinaturali/accesso-ai-dati/annali_meteoidrologici/annali-meteo-idro/banca-dati-idrologica.html
[3]http://www.idrologia.polito.it/didattica/PIT/2013/2_AnalisiRegionale/AltroMateriale/DATI_AtlanteBaciniImbriferi.pdf
[4]Data: ARPA Piemonte: NWIOI daily data, Version 2.1, data updated daily. Retrieved online from Rischi Naturali Archive Center, http://www.arpa.piemonte.it/rischinaturali/tematismi/clima/confronti-storici/dati/dati.html
Method: ARPA Piemonte: Metodologia dell'Optimal Interpolation, Tech. rep., Arpa Piemonte, Dipartimento Sistemi Previsionali, retrieved online from http://rsaonline.arpa.piemonte.it/meteoclima50/pdf/metodologia.pdf

Acquaotta, F., Fratianni, S., Garzena, D., 2015. Temperature changes in the North-Western Italian Alps from 1961 to 2010. Theoretical and Applied Climatology, 122, 619–634. https://doi.org/10.1007/s00704-014-1316-7

Alfieri, L., Burek, P., Feyen, L., Forzieri, G., 2015. Global warming increases the frequency of river floods in Europe. Hydrology and Earth System Sciences, 19, 2247–2260. https://doi.org/10.5194/hess-19-2247-2015

Barker, L., Hannaford, J., Muchan, K., Turner, S., and Parry, S., 2016. The winter 2015/2016 floods in the UK: a hydrological appraisal. Weather, 71, 324–333. https://doi.org/10.1002/wea.2822

Beniston, M., Farinotti, D., Stoffel, M., Andreassen, L.M., Coppola, E., Eckert, N., Fantini, A., Giacona, F., Hauck, C., Huss, M., Huwald, H., Lehning, M., López-Moreno, J.-I., Magnusson, J., Marty, C., Morán-Tejéda, E., Morin, S., Mohamed, N., Provenzale, A., Rabatel, A., Six, D., Stötter, J., Strasser, U., Terzago, S., Vincent, C., 2018. The European mountain cryosphere: a review of its current state, trends, and future challenges. The Cryosphere, 12, 2, 759–794. https://doi.org/10.5194/tc-12-759-2018

Bertola, M., Viglione, A., Blöschl, G., 2019. Informed attribution of flood changes to decadal variation of atmospheric, catchment and river drivers in Upper Austria. Journal of Hydrology, 577, 123919. https://doi.org/10.1016/j.jhydrol.2019.123919.

Bertola, M., Viglione, A., Lun, D., Hall, J., Blöschl, G., 2020. Flood trends in Europe: are changes in small and big floods different? Hydrology and Earth System Sciences, 24, 4, 1805–1822. https://doi.org/10.5194/hess-24-1805-2020

Bertola, M., Viglione, A., Vorogushyn, S., Lun, D., Merz, B., Blöschl, G., 2021. Do small and large floods have the same

drivers of change? A regional attribution analysis in Europe. Hydrology and Earth System Sciences, 25, 3, 1347–1364. https://doi.org/10.5194/hess-25-1347-2021

Best, D.J., Roberts, D.E., 1975. Algorithm AS 89: the upper tail probabilities of Spearman's rho. Journal of the Royal Statistical Society, Series C (Applied Statistics), 24, 3, 377–379.

Blöschl, G., Nester, T., Komma, J., Parajka, J., Perdigão, R.A.P., 2013a. The June 2013 flood in the Upper Danube Basin, and comparisons with the 2002, 1954 and 1899 floods. Hydrology and Earth System Sciences, 17, 5197–5212. https://doi.org/10.5194/hess-17-5197-2013

Blöschl, G., Sivapalan, M., Wagener, T., Savenije, H., Viglione, A., 2013b. Runoff Prediction in Ungauged Basins: Synthesis across Processes, Places and Scales. Cambridge University Press. ISBN: 978-1107028180

Blöschl, G., Hall, J., Parajka, J., Perdigão, R.A.P., Merz, B., Arheimer, B., Aronica, G.T., Bilibashi, A., Bonacci, O., Borga, M., Čanjevac, I., Castellarin, A., Chirico, G.B., Claps, P., Fiala, K., Frolova, N., Gorbachova, L., Gül, A., Hannaford, J., Harrigan, S., Kireeva, M., Kiss, A., Kjeldsen, T.R., Kohnová, S., Koskela, J.J., Ledvinka, O., Macdonald, N., Mavrova-Guirguinova, M., Mediero, L., Merz, R., Molnar, P., Montanari, A., Murphy, C., Osuch, M., Ovcharuk, V., Radevski, I., Rogger, M., Salinas, J.L., Sauquet, E., Šraj, M., Szolgay, J., Viglione, A., Volpi, E., Wilson, D., Zaimi, K., Živković, N., 2017. Changing climate shifts timing of European floods. Science, 357, 588–590. https://doi.org/10.1126/science.aan2506

Blöschl, G., Hall, J., Parajka, J., Perdigão, R.A.P., Merz, B., Arheimer, B., Aronica, G.T., Bilibashi, A., Bonacci, O., Borga, M., Čanjevac, I., Castellarin, A., Chirico, G. B., Claps, P., Fiala, K., Frolova, N., Gorbachova, L., Gül, A., Hannaford, J., Harrigan, S., Kireeva, M., Kiss, A., Kjeldsen, T.R., Kohnová, S., Koskela, J.J., Ledvinka, O., Macdonald, N., Mavrova-Guirguinova, M., Mediero, L., Merz, R., Molnar, P., Montanari, A., Murphy, C., Osuch, M., Ovcharuk, V., Radevski, I., Rogger, M., Salinas, J.L., Sauquet, E., Šraj, M., Szolgay, J., Viglione, A., Volpi, E., Wilson, D., Zaimi, K., Živković, N., 2019. Changing climate both increases and decreases European river floods. Nature, 573, 108–111. https://doi.org/10.1038/s41586-019-1495-6

Cassardo, C., Cremonini, R., Gandini, D., Paesano, G., Pelosini, R., Qian, M.W., 2001. Analysis of the severe flood (13-16 October 2000) in Piedmont (Italy). In: Proc. Conference on Environmental change and water sustainability, July 2001, Zaragoza, Spain.

Conover, W.J., 1999. Practical Nonparametric Statistics. 3rd Ed. John Wiley and Sons, New York, 493 p.

Desai, B., Maskrey, A., Peduzzi, P., De Bono, A., Herold, C., 2015. Making Development Sustainable: The Future of Disaster Risk Management. Global Assessment Report on Disaster Risk Reduction http://archive-ouverte.unige.ch/unige:78299 (UNISDR, 2015).

Doorenbos, J., Pruitt, W.O., 1977. Crop water requirements. FAO Irrigation and Drainage Paper No. 24. Food and Agriculture Organization of the United Nations, Rome. https://www.fao.org/3/f2430e/f2430e.pdf

Falkenmark, M., Chapman, T., 1989. Comparative hydrology: An ecological approach to land and water resources. The Unesco Press, Paris.

Farr, T.G., Rosen, P.A., Caro, E., Crippen, R., Duren, R., Hensley, S., Kobrick, M., Paller, M., Rodriguez, E., Roth, L., Seal, D., Shaffer, S., Shimada, J., Umland, J., Werner, M., Oskin, M., Burbank, D., Alsdorf, D., 2007. The shuttle radar topography mission. Reviews of Geophysics, 45, RG2004. https://doi.org/10.1029/2005RG000183

Fioravanti, G., Piervitali, E., Desiato, F., 2016. Recent changes of temperature extremes over Italy: an index-based analysis. Theoretical and Applied Climatology, 123, 3–4, 473–486. https://doi.org/10.1007/s00704-014-1362-1

Grazzini, F., Fragkoulidis, G., Pavan, V., Antolini, G., 2020. The 1994 Piedmont flood: an archetype of extreme precipitation events in northern Italy. Bulletin of Atmospheric Science and Technology, 1, 3, 283–295. https://doi.org/10.1007/s42865-020-00018-1

Hall, J., Arheimer, B., Aronica, G.T., Bilibashi, A., Boháč, M., Bonacci, O., Borga, M., Burlando, P., Castellarin, A., Chirico, G.B., Claps, P., Fiala, K., Gaál, L., Gorbachova, L., Gül, A., Hannaford, J., Kiss, A., Kjeldsen, T., Kohnová, S., Koskela, J.J., Macdonald, N., Mavrova-Guirguinova, M., Ledvinka, O., Mediero, L., Merz, B., Merz, R., Molnar, P., Montanari, A., Osuch, M., Parajka, J., Perdigão, R.A.P., Radevski, I., Renard, B., Rogger, M., Salinas, J.L., Sauquet, E., Šraj, M., Szolgay, J., Viglione, A., Volpi, E., Wilson, D., Zaimi, K., Blöschl, G., 2015. A European Flood Database: facilitating comprehensive flood research beyond administrative boundaries. Proceedings IAHS, 370, 89–95. https://doi.org/10.5194/piahs-370-89-2015

Helsel, D.R., Hirsch, R.M., Ryberg, K.R., Archfield, S.A., Gilroy, E.J., 2020. Statistical methods in water resources: U.S. Geological Survey Techniques and Methods, book 4, chapter A3, 458 p. https://doi.org/10.3133/tm4a3. [Supersedes USGS Techniques of Water-Resources Investigations, book 4, chapter A3, version 1.1.]

Hollander, M., Wolfe, D.A., 1999. Nonparametric Statistical Methods. John Wiley and Sons, New York, 787 p.

Kendall, M.G., 1975. Rank Correlation Methods. 4th Ed. Charles Griffin, London.

Kreienkamp, F., Philip, S.Y., Tradowsky, J.S., Kew, S.F., Lorenz, P., Arrighi, J., Belleflamme, A., Bettmann, T., Caluwaerts, S., Chan, S.C., Ciavarella, A., De Cruz, L., De Vries, H., Demuth, N., Ferrone, A., Fischer, E.M., Fowler, H.J., Goergen, K., Heinrich, D., Henrichs, Y., Lenderink, G., Kaspar, F., Nilson, E., Otto, F.E.L., Ragone, F., Seneviratne, S.I., Singh, R.K., Skålevåg, A., Termonia, P., Thalheimer, L., Van Aalst, M., Van den Bergh, J., Van de Vyver, H., Vannitsem, S., Van Oldenborgh, G.J., Van Schaeybroeck, B., Vautard, R., Vonk, D., Wanders, N., 2021. Rapid attribution of heavy rainfall events leading to the severe flooding in Western Europe during July 2021. https://www.worldweatherattribution.org/wp-content/uploads/Scientific-report-Western-Europe-floods-2021-attribution.pdf

Libertino, A., Ganora, D., Claps, P., 2019. Evidence for increasing rainfall extremes remains elusive at large spatial scales: The case of Italy. Geophysical Research Letters, 46, 13, 7437–7446. https://doi.org/10.1029/2019GL083371

Lun, D., Viglione, A., Bertola, M., Komma, J., Parajka, J., Valent, P., Blöschl, G., 2021. Characteristics and process controls of statistical flood moments in Europe – a data based analysis. Hydrology and Earth System Sciences, 25, 5535–5560. https://doi.org/10.5194/hess-25-5535-2021

Mann, H.B., 1945. Non-parametric tests against trend. Econometrica, 13, 245–259.

Mediero, L., Santillán, D., Garrote, L., Granados, A., 2014. Detection and attribution of trends in magnitude, frequency and timing of floods in Spain. Journal of Hydrology, 517, 1072–1088. https://doi.org/10.1016/j.jhydrol.2014.06.040

Merz, R., Blöschl, G., 2003. A process typology of regional floods. Water Resources Research, 39, 1–20. https://doi.org/10.1029/2002WR001952,

http://doi.wiley.com/10.1029/2002WR001952

Merz, R., Blöschl, G., 2005. Flood frequency regionalization–spatial proximity vs. catchment attributes. Journal of Hydrology, 302, 1–4, 283–306. https://doi.org/10.1016/j.jhydrol.2004.07.018

Miller, J.D., Kjeldsen, T.R., Hannaford, J., Morris, D.G., 2013. A hydrological assessment of the November 2009 floods in Cumbria, UK. Hydrology Research, 44, 180–197. https://doi.org/10.2166/nh.2012.076

Peterson, T.C., 2005. Climate Change Indices. WMO Bulletin, 54, 2, 83–86.

Petrow, T., Merz, B., 2009. Trends in flood magnitude, frequency and seasonality in Germany in the period 1951–2002. Journal of Hydrology, 371, 129–141. https://doi.org/10.1016/j.jhydrol.2009.03.024

Prosdocimi, I., Kjeldsen, T.R., Svensson, C., 2014. Non-stationarity in annual and seasonal series of peak flow and precipitation in the UK. Natural Hazards and Earth System Sciences, 14, 1125–114. https://doi.org/10.5194/NHESS-14-1125-2014

Prosdocimi, I., Kjeldsen, T.R., Miller, J.D., 2015. Detection and attribution of urbanization effect on flood extremes using non-stationary flood-frequency models. Water Resources Research, 51, 4244–4262. https://doi.org/10.1002/2015WR017065

Rojas, R., Feyen, L., Bianchi, A., Dosio, A., 2012. Assessment of future flood hazard in Europe using a large ensemble of bias corrected regional climate simulations. Journal of Geophysical Research - Atmospheres, 117, D17109. https://doi.org/10.1029/2012JD017461

Sardella, A., Palazzi, E., Hardenberg, J.V., Grande, C.D., Nuntiis, P.D., Sabbioni, C., Bonazza, A., 2020. Risk Mapping for the Sustainable Protection of Cultural Heritage in Extreme Changing Environments. Atmosphere, 11, 7, 700. http://dx.doi.org/10.3390/atmos11070700

Sen, P.K., 1968. Estimates of the regression coefficient based on Kendall's tau. Journal of the American Statistical Association, 63, 324, 1379–1389.

Silvestro, F., Gabellani, S., Giannoni, F., Parodi, A., Rebora, N., Rudari, R., Siccardi, F., 2012. A hydrological analysis of the 4 November 2011 event in Genoa. Natural Hazards and Earth System Sciences, 12, 9, 2743–2752.

Silvestro F., Rebora, N., Rossi, L., Dolia, D., Gabellani, S., Pignone F., Masciulli, C., 2016. What if the 25 October 2011 event that struck Cinque Terre (Liguria) had happened in Genoa, Italy? Flooding scenarios, hazard mapping and damage estimation. Natural Hazards and Earth System Sciences, 16, 8, 1737–1753.

Šraj, M., Viglione, A., Parajka, J., Blöschl, G., 2016. The influence of non-stationarity in extreme hydrological events on flood frequency estimation. Journal of Hydrology and Hydromechanics, 64, 426–437. https://doi.org/10.1515/johh-2016-0032

Theil, H., 1950. A rank invariant method of linear and polynomial regression analysis. Proceedings of the Koninklijke Nederlandse Akademie Wetenschappen, Series A Mathematical Sciences, 53, 386-392.

Ulbrich, U., Brücher, T., Fink, A.H., Leckebusch, G.C., Krüger, A., Pinto, J.G., 2003. The central European floods of August 2002: Part 1 – Rainfall periods and flood development. Weather, 58, 371–377. https://doi.org/10.1256/wea.61.03A

Viglione, A., Merz, B., Viet Dung, N., Parajka, J., Nester, T., Blöschl, G., 2016. Attribution of regional flood changes based on scaling fingerprints. Water Resources Research, 52, 5322–5340. https://doi.org/10.1002/2016WR019036

Villarini, G., Smith, J.A., Serinaldi, F., Ntelekos, A.A., 2011. Analyses of seasonal and annual maximum daily discharge records for central Europe. Journal of Hydrology, 399, 299–312. https://doi.org/10.1016/j.jhydrol.2011.01.007

Zeng, X., Schnier, S., Cai X., 2021. A data-driven analysis of frequent patterns and variable importance for streamflow trend attribution. Advances in Water Resources, 147, 103799. https://doi.org/10.1016/j.advwatres.2020.103799

Zhang, X., Hegerl, G., Zwiers, F.W., Kenyon, J., 2005. Avoiding inhomogeneity in percentile-based indices of temperature extremes. Journal of Climate, 18, 11, 1641–1651. https://doi.org/10.1175/JCLI3366.1

APPENDIX

Table A1. Regional mean Spearman's correlation coefficients, weighted for the uncertainty bounds, among precipitation ETCCDI indices and annual maximum mean daily discharges. The percentage of significant cases for each index is also reported.

Precipitation Index	Definition	Regional mean Spearman's correlation coefficient	Percentage of significant cases (one-sided test, α = 0.05)
Rx5day	Maximum 5-day precipitation [mm]	0.729	81%
R99pTOT	Annual total precipitation when daily precipitation is greater than the 99th percentile [mm]	0.659	78%
Rx1day	Maximum 1-day precipitation [mm]	0.657	76%
R95pTOT	Annual total precipitation when daily precipitation is greater than the 95th percentile [mm]	0.578	65%
SDII	Simple precipitation intensity index [mm/day]	0.539	66%
PRCPTOT	Annual total precipitation in wet days [mm]	0.417	43%
R20mm	Annual number of days with precipitation > 20 mm [days]	0.343	33%
R10mm	Annual number of days with precipitation > 10 mm [days]	0.205	21%
CWD	Maximum length of wet spell (number of consecutive wet days) [days]	0.193	19%
CDD	Maximum length of dry spell (number of consecutive dry days) [days]	− 0.192	18%
R1mm	Annual number of wet days [days]	0.053	15%

Table A2. Regional mean Spearman's correlation coefficients, weighted for the uncertainty bounds, among temperature ETCCDI indices and annual maximum mean daily discharges. The percentage of significant cases for each index is also reported. * refer to the webpage for a complete definition.

Temperature Index	Definition	Regional mean Spearman's correlation coefficient	Percentage of significant cases (one-sided test, α = 0.05)
TR	Number of tropical nights (daily minimum temperature > 20 °C)	0.353	23%
TNx	Annual maximum value of daily minimum temperature	0.304	18%
TXx	Annual maximum value of daily maximum temperature	0.283	27%
SU	Number of summer days (daily maximum temperature > 25 °C)	0.252	19%
TXn	Annual minimum value of daily maximum temperature	− 0.187	19%
ID	Number of icing days (daily maximum temperature < 0 °C)	0.141	13%
TNn	Annual minimum value of daily minimum temperature	− 0.127	13%
DTR	Daily temperature range (annual mean difference between daily maximum and minimum temperature)	0.106	6.3%
FD	Number of frost days (daily minimum temperature < 0 °C)	0.098	9.5%
WSDI	Warm spell duration index (number of days with at least 6 consecutive days when daily maximum temperature > 90th percentile)	0.090	10.5%
GSL	Growing season length*	− 0.085	9.5%
CSDI	Cold spell duration index (number of days with at least 6 consecutive days when daily minimum temperature < 10th percentile)	0.077	10.5%
TX90p	% of days when daily maximum temperature > 90th percentile	0.071	8.4%
TN10p	% of days when daily minimum temperature < 10th percentile	0.050	14%
TN90p	% of days when daily minimum temperature > 90th percentile	0.034	7.3%
TX10p	% of days when daily maximum temperature < 10th percentile	0.013	7.3%

Table A3. Regional mean Spearman's correlation coefficients, weighted for the uncertainty bounds, among detrended series of precipitation ETCCDI indices and annual maximum mean daily discharges. The percentage of significant cases for each index is also reported.

Precipitation Index	Definition	Regional mean Spearman's correlation coefficient	Percentage of significant cases (one-sided test, $\alpha = 0.05$)
Rx5day	Maximum 5-day precipitation [mm]	0.728	84%
Rx1day	Maximum 1-day precipitation [mm]	0.683	78%
R99pTOT	Annual total precipitation when daily precipitation is greater than the 99th percentile [mm]	0.667	80%
R95pTOT	Annual total precipitation when daily precipitation is greater than the 95th percentile [mm]	0.579	64%
SDII	Simple precipitation intensity index [mm/day]	0.535	62%
PRCPTOT	Annual total precipitation in wet days [mm]	0.386	39%
R20mm	Annual number of days with precipitation > 20 mm [days]	0.311	29%
CWD	Maximum length of wet spell (number of consecutive wet days) [days]	0.172	17%
CDD	Maximum length of dry spell (number of consecutive dry days) [days]	− 0.165	17%
R10mm	Annual number of days with precipitation > 10 mm [days]	0.156	20%
R1mm	Annual number of wet days [days]	0.002	14%

Table A4. Regional mean Spearman's correlation coefficients, weighted for the uncertainty bounds, among detrended series of temperature ETCCDI indices and annual maximum mean daily discharges. The percentage of significant cases for each index is also reported. * refer to the webpage for a complete definition.

Temperature Index	Definition	Regional mean Spearman's correlation coefficient	Percentage of significant cases (one-sided test, $\alpha = 0.05$)
TR	Number of tropical nights (daily minimum temperature > 20 °C)	0.360	23%
TXx	Annual maximum value of daily maximum temperature	0.330	37%
TNx	Annual maximum value of daily minimum temperature	0.318	21%
SU	Number of summer days (daily maximum temperature > 25 °C)	0.260	18%
TXn	Annual minimum value of daily maximum temperature	− 0.231	26%
ID	Number of icing days (daily maximum temperature < 0 °C)	0.171	12%
TNn	Annual minimum value of daily minimum temperature	− 0.146	16%
FD	Number of frost days (daily minimum temperature < 0 °C)	0.142	12%
GSL	Growing season length*	− 0.134	13%
TN10p	% of days when daily minimum temperature < 10th percentile	0.106	16%
TN90p	% of days when daily minimum temperature > 90th percentile	0.086	17%
CSDI	Cold spell duration index (number of days with at least 6 consecutive days when daily minimum temperature < 10th percentile)	0.083	20%
DTR	Daily temperature range (annual mean difference between daily maximum and minimum temperature)	0.082	9.5%
WSDI	Warm spell duration index (number of days with at least 6 consecutive days when daily maximum temperature > 90th percentile)	0.077	15%
TX10p	% of days when daily maximum temperature < 10th percentile	0.068	12%
TX90p	% of days when daily maximum temperature > 90th percentile	0.068	9.5%

Table A5. Regional mean trends of precipitation ETCCDI indices and annual maximum discharges, weighted for the uncertainty bounds. The percentage of significant cases for each index is also reported.

Precipitation Index	Definition	Regional mean trend (% of mean per year)	Percentage of significant cases (one-sided test, α = 0.05)
R99pTOT	Annual total precipitation when daily precipitation is greater than the 99th percentile [mm]	3.277	17%
R95pTOT	Annual total precipitation when daily precipitation is greater than the 95th percentile [mm]	2.981	27%
R20mm	Annual number of days with precipitation > 20 mm [days]	1.917	48%
PRCPTOT	Annual total precipitation in wet days [mm]	1.603	48%
Rx5day	Maximum 5-day precipitation [mm]	1.590	9.5%
R10mm	Annual number of days with precipitation > 10 mm [days]	1.506	40%
Rx1day	Maximum 1-day precipitation [mm]	1.186	9.5%
SDII	Simple precipitation intensity index [mm/day]	1.136	41%
CDD	Maximum length of dry spell (number of consecutive dry days) [days]	− 0.334	10.5%
R1mm	Annual number of wet days [days]	0.282	3.2%
CWD	Maximum length of wet spell (number of consecutive wet days) [days]	0.249	2.1%
Qmax	Annual maximum mean daily discharge [m^3/s]	0.873	7.4%

Table A6. Regional mean trends of temperature ETCCDI indices, weighted for the uncertainty bounds. The percentage of significant cases for each index is also reported. *refer to the webpage for a complete definition.

Temperature Index	Definition	Regional mean trend (% of mean per year)	Percentage of significant cases (one-sided test, α = 0.05)
WSDI	Warm spell duration index (number of days with at least 6 consecutive days when daily maximum temperature > 90th percentile)	4.341	55%
TX10p	% of days when daily maximum temperature < 10th percentile	− 4.303	76%
TN10p	% of days when daily minimum temperature < 10th percentile	− 3.335	62%
TX90p	% of days when daily maximum temperature > 90th percentile	2.901	54%
TN90p	% of days when daily minimum temperature > 90th percentile	2.483	52%
ID	Number of icing days (daily maximum temperature < 0 °C)	− 2.027	16%
SU	Number of summer days (daily maximum temperature > 25 °C)	1.775	32%
TR	Number of tropical nights (daily minimum temperature > 20 °C)	1.480	36%
FD	Number of frost days (daily minimum temperature < 0 °C)	− 1.299	24%
TXn	Annual minimum value of daily maximum temperature	1.277	2.1%
CSDI	Cold spell duration index (number of days with at least 6 consecutive days when daily minimum temperature < 10th percentile)	− 0.996	32%
TNn	Annual minimum value of daily minimum temperature	0.611	1%
TNx	Annual maximum value of daily minimum temperature	0.534	35%
TXx	Annual maximum value of daily maximum temperature	0.382	30%
DTR	Daily temperature range (annual mean difference between daily maximum and minimum temperature)	0.334	40%
GSL	Growing season length*	0.096	17%